Structural analysis of neutron-irradiated $(Ba_{0.88}Ca_{0.12}Ti_{0.975}Sn_{0.025})O_3$ ceramic

Umaru Ahmadu[1], Abdulwaliyu B. Usman[1], Auwal M. Muhammad[2], Oyeleke I. Olarinoye[1], Moses Agida[1]

[1]*Department of Physics, Federal University of Technology, P.M.B., 65, Minna, Nigeria*
[2]*Centre for Energy Research and Training (CERT), Ahmadu Bello University, Zaria, Nigeria*

[*]Corresponding author: E-mail: u.ahmadu@yahoo.com

Received: 21 March 2016, Revised: 07 August 2016 and Accepted: 20 April 2017

DOI: 10.5185/amp.2017/565
www.vbripress.com/amp

Abstract

Co-doped barium calcium stannate titanate ($Ba_{0.88}Ca_{0.12}Ti_{0.975}Sn_{0.025}O_3$) ceramics, synthesized via solid state reaction and sintered at 1100 °C/3 h. The ceramics were irradiated with thermal neutrons of up to 1.4 × 1010 n/cm_2 using a 5 Ci Am-Be source having an average flux of 2.7 × 104 n/cm_2.s. Structural analysis of the ceramics indicate a majorly polycrystalline material with a minor secondary phase. The 2θ positions were observed to shift slightly to higher angles and the microstrain remained constant with increase in fluence. The average crystallite size is ~ 38 nm with anisotropy in lattice expansion observed. Rod-like grains, porous regions and agglomerations were observed in all the specimens. There was general increase in grain size with increase in fluence and the average grain size is ~1 μm. Chemical analysis indicates slight deviation from nominal ones for some irradiated samples. It is concluded that the structural and microstructural changes observed would not affect the performance of the devices based on this material when used in radiation environments of neutrons as the maximum fluence has not exceeded the order of magnitude of threshold for radiation damage.

Keywords: Ceramics, neutron irradiation, lattice parameters, grain size, nuclear reactors.

Introduction

Recently, Barium titanate ($BaTiO_3$ or BT), particularly under doping conditions, has had numerous applications across different sectors from energy to electronic components. It is used in multilayered ceramic capacitors (MLCCs) in devices [**1**] and its outstanding ferroelectric and piezoelectric properties are of great interest in sensors, microactuators and ferroelectric random-access memory (FeRAM), among others [**1, 2**]. BT has tetragonal crystal structure from room temperature up to the Curie temperature (Tc, 120 °C) above which its ferroelectric behavior disappears as it transforms into cubic phase [**2, 3**]. Similarly, it has low piezoelectric constants and structural instability sets in at a relatively low transition temperature (120 °C) which hampers its diverse applications [**4**]. Several methods/techniques have been developed to improve the structural stability, among other properties. These efforts include partial/whole substitutions of the Ba^{2+} or Ti^{4+} sites with ions of different or same charge and comparable sizes [**5-12**].

One of the significant applications of BT-based ceramics is in their application in devices such as actuators, sensors in particle accelerators and nuclear reactors in outer space environments which contain abundant nuclear radiation [**13, 14**]. Here, the major concern is in the stability of BT-based devices. Nuclear radiations, neutrons, are of special interest because they interact with the atomic nuclei of materials by causing atomic displacements, thereby dislodging atoms from their lattice sites [**15**]. This eventually results in the production of vacancy-interstitial pairs which subsequently lead to defects that can cause irreversible changes in the structural and electrical properties of BT-based ceramics. The extent of such damage depends on radiation parameters such as energy, dose, nature of the material and its structural phase [**16**]. Nuclear irradiations of BT-based ceramics have been established to alter the piezoelectric, dielectric and microstructural and structural properties [**13, 14, 17, 18**]. The earliest work reported in this regard is on single crystalline BT irradiated at about 100 °C with an integrated fast neutron flux of 1.8 × 10^{20} n/cm^2 in which it was observed that the tetragonal single crystals had been transformed to perovskite-type cubic single crystal normally stable at 120 °C. Measurements of lattice parameters indicated anisotropic expansion had occurred [**17**]. In another

study, the ferroelectric character of BT and BT-type materials were altered significantly after pile irradiation of between 1×10^{15} n/cm^2 and 1×10^{18} n/cm^2 with decrease in dielectric constant and shifts in lattice constants observed [**18**]. Other authors have reported the radiation damage threshold of some pressure transducers constructed using BT as 7.6×10^{10} n/cm^2 for bulk damage [**19**]. However, work on neutron irradiated co-doped BT ($Ba_{0.88}Ca_{0.12}Ti_{0.975}Sn_{0.025}O_3$) (BCST) is rarely found in literature to the best of our knowledge, though the present authors have reported work on gamma irradiation of the same compound [**20**]. In the present work, co-doping of BT by substitution of Ba^{2+} and Ti^{4+} sites with 0.12 mol of Ca^{2+} and 0.025 mol of Sn^{4+} at different levels of thermal neutron fluence was carried out. Substitution of Ba^{2+} by Ca^{2+} has been reported to effectively inhibit grain growth, improve electromechanical properties and the transition temperature which lead, eventually, to structural stability but decreased dielectric constant [**7-9**]. On the other hand, substitution of Ti^{4+} by Sn^{4+} leads to an increase in piezoelectric and dielectric properties and a decrease in transition temperature [**12**]. These simultaneous substitutions are expected to lead to structural stability fundamentally and to an improvement in other structure-dependent properties. Thus, results of structural and microstructural properties are presented.

Experimental

Materials

The precursor materials used for the synthesis and their details have been reported in our earlier work [**20**].

Material synthesis

Stoichiometric amounts of the materials were used for the synthesis using eqn. (1).

$$0.88BaCO_3+0.12CaCO_3+0.025SnO_2+0.975TiO_2 \downarrow Ba_{0\cdot88}Ca_{0\cdot12}Sn_{0\cdot02}Ti_{0\cdot975}O_3+CO_2 \quad (1)$$

Details of the preparation and synthesis conditions have been reported in our earlier work [**20**]. Meanwhile, sintered and pelletized samples were irradiated in a low neutron flux irradiation facility [**21**] which exists as a 750 mm by 800 mm paraffin cylinder having at its centre a 5 Ci Am-Be isotopic neutron source (diameter 30 mm, and height 48 mm.) with average thermal neutron flux of 2.7387×10^4 n/cm^2.s which has six irradiation ports arranged symmetrically around the source. These provide opportunity for simultaneous irradiation of six samples at a time. For this work, five groups of pellets of the samples were placed in a polythene bag and lowered into the ports with the aid of a thread. The pellets were irradiated at 8.1×10^6, 9.72×10^7, 8.75×10^8, 6.99×10^9 and 1.4×10^{10} neutron fluences. The samples were subsequently labelled as BCST-06, BCST-07, BCST-08, BCST-09 and BCST-10, respectively. To attain the required neutron fluences, the pellets were brought out after successive irradiation times of 6 mins, 1 hr, 9 hrs, 72 hrs and 144 hrs have elapsed. Literature survey revealed that BT has a flux threshold of 2.1×10^4 n/cm^2.s and experiences bulk damage at neutron fluence of 7.6×10^{10} n/cm^2 [**19**]. This informed the choice of the neutron fluences used in the present study. The neutron fluences were determined using eqn. (2).

$$\Phi = \int \phi(t)\, dt \quad (2)$$

where, the neutron fluence (Φ) is the neutron flux integrated over a certain time period and $\phi(t)$ is the neutron flux in n/cm^2.s while *dt* is the time period of exposure in seconds.

Characterization

X-ray Diffractometer (D8 Advance, BRUKER AXS, 40 kV, 40 mA) with monochromatic CuKα (λ = 1.54060 Å) over a step scan mode of step size 0.034 ° and counts accumulated for 88 s at each step for 2θ values ranging from 20 ° to 90 ° was used to characterize the structural phase composition of the pristine and irradiated ceramics. The ceramics were mounted on an aluminum stage with the aid of carbon adhesive tape and coated with AuPd (Gold-Palladium) using a sputter coater. High Resolution Scanning Electron Microscope (HRSEM, Zeiss) coupled with an Energy Dispersive Spectrometer (EDS) was employed to record and analyze the surface morphology and elemental compositions of the pristine and irradiated ceramics. The instrument was operated at a voltage of 20 kV and images were captured at 5 kV.

Results and discussion

Crystal structure parameters

X-ray Diffraction (XRD) patterns of the synthesized BCST ceramics at room temperature exposed to different neutron fluence are depicted in **Fig. 1**. The noticeable peaks in the XRD spectra indicated that the pristine and irradiated BCST ceramics are polycrystalline which compares well with JCPDS no: 00-005-0626 file for tetragonal phase $BaTiO_3$. However, a minor peak around 47.5° 2θ was observed and identified as orthorhombic $CaTiO_3$ phase (JCPDS file no: 00-022-0153). Other diffraction peaks are evident though with very low intensities whose match could not be found as shown in the XRD spectra.

The XRD patterns of the irradiated ceramics suggest a consistent phase and composition with the

pristine sample. This suggests that neutron did not deteriorate the perovskite structure of barium titanate based ceramics over the range of fluence studied.

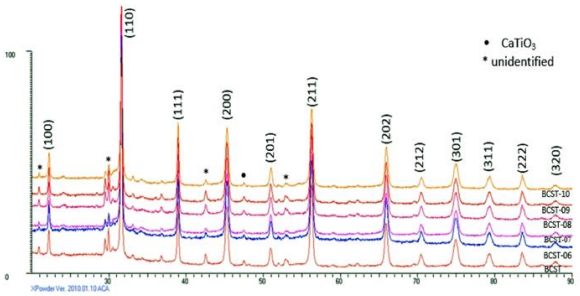

Fig.1. X-ray diffraction patterns of as-sintered and irradiated $(Ba_{0.88}Ca_{0.12}Ti_{0.975}Sn_{0.025})O_3$ ceramics.

Table 1. Samples, peak positions (*2θ*) at **(**200), d-spacings (*d*) and the microstrain (*ε)* of as-sintered and irradiated BCST ceramics.

Sample	2θ (degree)	*d* (Å)	Microstrain ($\varepsilon \times 10^{-3}$)
BCST	45.261	2.00189	3.2
BCST-06	45.283	2.00097	3.1
BCST-07	45.278	2.00117	3.2
BCST-08	45.281	2.00106	3.3
BCST-09	45.285	2.00088	3.2
BCST-10	45.293	2.00054	3.1

Table 1 shows the experimentally determined and computed parameters for the samples. It is observed that the 200 peak which is the structure sensitive peak slightly shifts towards higher 2θ angles with increase in fluence level compared to pristine sample, while the corresponding *d*-values remain constant (as expected) for the same peak irrespective of level of fluence. Substitutions at the A-site of perovskite materials by ions of smaller size have been linked to changes in unit cell lattice parameters [**22, 23**]. Similarly, the slight shifts of the peaks may be attributed to A-site defect induced by neutrons. However, the microstrain values calculated using eqn. (3) [**24**], appear to be near constant before and after irradiation. This suggests that the microstrain induced because of irradiation is insignificant and radiation independent. However, ferroelectric and dielectric properties of BT-based ceramics are reported to decrease when microstrain increases because of their link [**13, 14**]. This parameter thus shows that these two properties are unchanged.

$$\varepsilon = \frac{\beta}{4\tan\theta} \tag{3}$$

where, ε is the microstrain, θ the Bragg diffraction angle, and β the full width at half maximum (FWHM).

The calculated average crystallite sizes using the most intense peak for all the samples and determined from eqn. (4) [**25**] is approximately 38 nm. It can be observed from the plot of τ (average crystallite size) against irradiation fluence (**Fig. 2**) that average crystallite sizes generally increased with increase in level of fluence. The increase in τ values after neutron exposure is due to oxygen vacancies induced by the neutrons [**26-28**]. The result also suggests an increase in level of crystallization as corroborated in the decrease in β in **Fig. 2.**

$$\tau = \frac{0.9\lambda}{\beta\cos\theta} \tag{4}$$

where, β is the FWHM of the diffraction peak in radians, θ the Bragg diffraction angle, λ the wavelength of the X-ray used and τ the average crystallite size in nanometers.

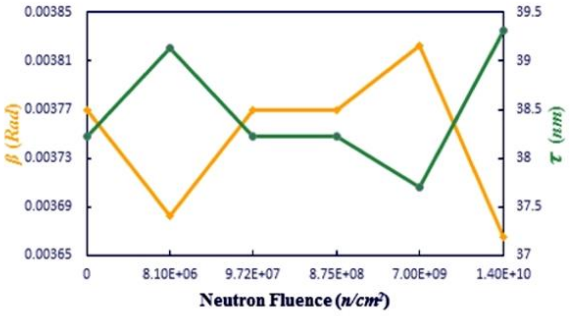

Fig. 2. Variation of β and τ against neutron fluence.

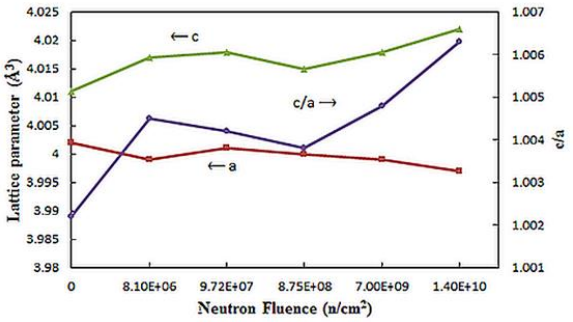

Fig. 3. Variation of lattice parameters *a*, *c* and *c/a* ratio with neutron fluence.

The lattice constants *a* and *c* of the pristine and irradiated ceramics were calculated from the XRD data using 100, 200 and 201 diffraction peaks. The calculated *c/a* ratio (1.0022) of the tetragonal phase of the pristine sample shows that it is weakly tetragonal in contrast with the JCPDS reference data of $BaTiO_3$ (*c/a* = 1.0110) prepared at higher temperature. **Fig. 3** depicts the plot of the lattice constants and *c/a* ratio versus neutron fluence. Generally, there is decrease in *a* values with increase in fluence while *c* values generally increased. Similarly, the *c/a* ratio generally increased too. This imply an increase in tetragonality of the BCST ceramics upon exposure making it less prone to get center of symmetry which typically takes away the

tetragonality of perovskite titanates and subsequently leads to loss of ferroelectric and piezoelectric characteristics. Increase in *c/a* ratio leads to increase in polarizability which results in increased ferroelectric properties [**29**]. Therefore, it is expected that irradiation would not alter the ferroelectric properties of the BCST ceramics. These analyses indicate that despite the variations, the ceramics retain essentially the ferroelectric and piezoelectric properties.

Variations observed in the lattice parameters are due to displacements of host atoms upon energy exchange with the neutrons which have been found to lead to lattice distortion and anisotropic expansion [**17, 30**]. This is consistent with the slight shift in peak positions to higher 2θ values. These changes support the observation that the structural phase of BCST ceramic remains unchanged after irradiation and this is obvious from the XRD patterns. Overall, it is expected that the ferroelectric, piezoelectric and polarizability will remain the same or there would be a slight increment.

The anisotropic lattice expansion observed in the ceramics implies changes in cell volume. For the pristine specimen, the calculated value was found to be 64.20 $Å^3$ which subsequently increased by 0.123 %, 0.025 % and 0.025 % in BCST-07, BCST-09 and BCST-10, respectively, after irradiation. BCST-06 slightly decreased in value by 0.002% and is due to interstitial ions or ions larger in size because of their displacement from lattice sites by neutrons [**28, 30**].

Microstructural characterization

The results of microstructural characterizations of pristine and irradiated specimens of the ceramics are shown in **Fig. 4**(a-f). The microstructure in **Fig. 4** (b, e) are relatively brighter than the others and might be due to strong reflection in the visible region but has not been reported. There is non-uniform distribution of grains and agglomerations because of clustering in all the specimens and some porous regions are apparent.

which agrees well with the XRD results of crystallite size which are found to increase in fluence, except for BCST-08 which decreased. Ferroelectric and dielectric properties are expected to increase with increase in grain size [**10, 13, 14**].

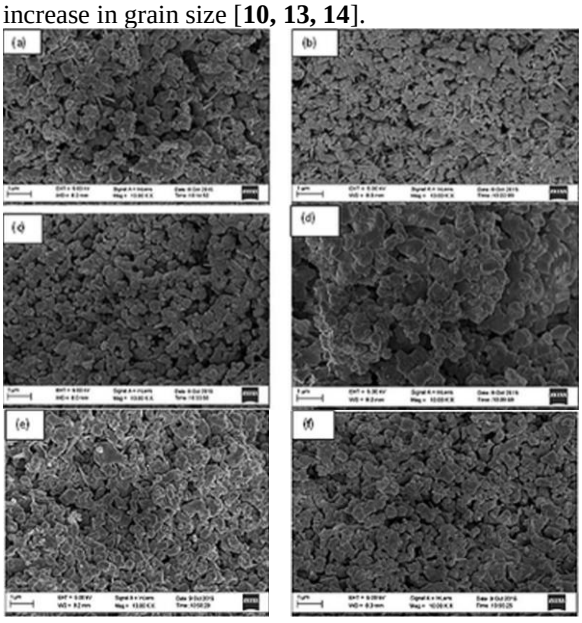

Fig. 4. HRSEM micrographs of (a) as-sintered (b) BCST-06 (c) BCST-07 (d) BCST-08 (e) BCST-09 and (f) BCST-10.

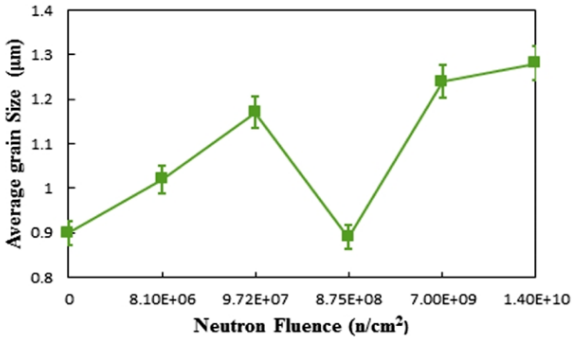

Fig. 5. Variation of grain size of BCST ceramic with neutron fluence.

Table 2. Elemental composition of pristine and irradiated BCST ceramics.

	Nominal Composition [at. %]						Normalized EDS derived Composition [at. %]							
Sample	**Ba**	**Ca**	**Sn**	**Ti**	**O**	**Total**	**Ba**	**Ca**	**Sn**	**Ti**	**O**	**Al**	**Ce**	**Total**
BCST	17.60	2.40	0.50	19.50	60.00	100	22.31	4.70	0.40	26.64	45.95	-	-	100
BCST-06	17.60	2.40	0.50	19.50	60.00	100	19.78	3.51	0.63	23.08	53.04	-	-	100
BCST-07	17.60	2.40	0.50	19.50	60.00	100	16.53	3.05	0.51	20.02	58.92	0.97	-	100
BCST-08	17.60	2.40	0.50	19.50	60.00	100	17.50	3.35	0.42	19.15	58.90	0.68	-	100
BCST-09	17.60	2.40	0.50	19.50	60.00	100	16.26	2.67	0.47	19.59	59.36	0.74	0.88	100
BCST-10	17.60	2.40	0.50	19.50	60.00	100	21.22	5.83	0.59	25.02	46.56	0.78	-	100

The average grain size determined using Imagej software for about 100 grains is ~1 µm (**Fig. 5**) and is smaller than those observed in traditional BT ceramics sintered at higher temperature (1450°C) [**19**]. Rod-like grains are also visible which reduces drastically with increased fluence. There is increase in average grain size with increase in fluence level

Chemical composition

Qualitative and quantitative EDS analysis for the pristine and irradiated samples show similar chemical compositions. **Fig. 6** is a representative EDS spectrum of the pristine BCST ceramic as they are all similar, while **Table 2** is the result of the

quantification analysis. The spectrum reveals the presence of Ba, Ca, Ti, Sn, O, C, Au and Pd. The carbon (C) is attributed to the carbon tape background while the AuPd (Gold-Paladium) is from the coating used to make it conduct for the measurement. **Table 2** also shows the quantitative comparison of nominal and EDS derived compositions of pristine and irradiated BCST ceramics where the elements have been normalized to 100%. There is evidence of Al impurity in virtually all the irradiated ceramics except in BCST-06 and BCST-09 in which Ce is additionally present in the latter. Presence of Al could be attributed to contamination during the process of irradiation. The presence of Ce cannot be explained at this time. Generally, the normalized EDS results are higher compared to the nominal ones. This is attributed to the displacement of lattice atoms to interstitials sites which, commutatively, lead to clustering and eventually manifests itself in inhomogeneities. Further, oxygen deficiency in the ambient during sintering can also lead to this discrepancy [**31**]. The overlap seen in Ba and Ti makes it difficult to differentiate between them in the quantification results and has been reported [**32**].

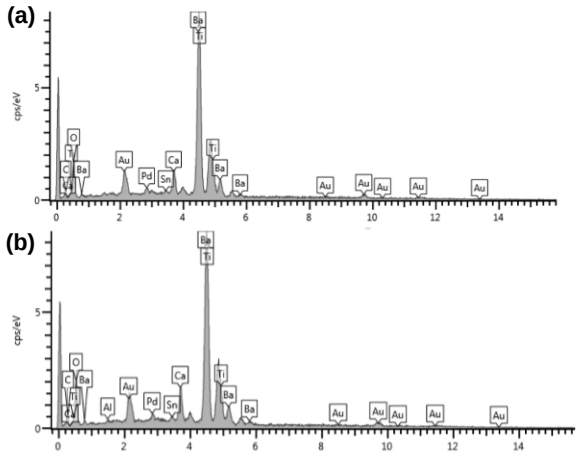

Fig. 6. EDS spectrum of (a) pristine BCST ceramic (b) irradiated BCST ceramic.

Conclusion

The Slight shifts were observed in 2θ peak positions to higher values with increase in fluence level. The observed microstrain are insignificant and irradiation independent. Increase in crystallite size was observed as neutron fluence increased and the average crystallite size was calculated to be ~38 nm. This suggests a slight increase in crystallization. The lattice parameters (a and c) show slight anisotropic expansion and the c/a ratio slightly increased and therefor imply that the piezoelectric, ferroelectric and polarizability properties might slightly increase or remain the same. A general increase in unit cell volume was observed and the microstructure of some of the irradiated specimens looks brighter relative to the pristine specimen and some of the irradiated ones. Non-uniform distribution of grains, rod-like grains, porous regions and agglomerations were observed in all the specimens at differing degrees. There is generally an increase in grain size (average ~1.0 μm) as the fluence level increased with the ferroelectric and dielectric properties expected to increase as a result. Chemical analysis (EDS) showed that all the nominal elements are present except the presence of some impurities which were generally accounted for. Higher concentrations of elements were obtained for EDS-derived measurements and are due to defects resulting in inhomogeneities in the microstructure, among others. Overall, the result shows that although there are some slight changes in structural and microstructural properties, the essential physical properties of the BT-based material, i.e, piezoelectric, ferroelectric and dielectric properties remain virtually the same and thus device performance is expected to be stable.

Acknowledgements

This work was funded by the Tertiary Education Trust Fund (TETFUND) under project no: TETFUND/FUTMINNA/'2014/044.

References

1. Heng, W.; Xinhua, Z. (2016). Perovskite Oxide Nanocrystals-Synthesis, Characterization, Functionalization, and Novel Applications; Likun P. (Ed.); InTech, **2016**, pp 155-170.
2. Nada, F. A.; Ahmed, G.; Ekram, H.E. Perovskite Nanomaterials-Synthesis, Characterization, and Applications; Likun P. (Ed.); InTech, **2016**, pp 111-112.
3. Frattini, A., Di Loreto, A., de Sanctis, O., Benavidez, E; *Procedia Mater Sci;* **2012**, 359-360.
4. Aksel, E.; Jones, J.L; *Sensors;* **2010**, 10, 1935-1954.
5. Vitayakorn, N; *J. Appl. Sci Res;* **2006,** 2(12), 1319-1322.
6. Rao, M. V. S.; Ramesh, V. K.; Rames, M.N.V.; Rao, B.S; *Adv. Mate. Phys. Chem.*, **2013**, 3, 77-82.
7. Choi, Y.K.; Hoshina, T.; Takeda, H.; Tsurumi, T; *J. Ceram. Soc. Jpn.*, **2010**,118, 881-886.
8. Matsuura, K.; Hoshina, T.; Takeda, H.; Sakabe, Y.; Tsurumi, T; *J. Ceram. Soc. Jpn*., **2014**, 122, 402-405.
9. Paunovic, V.; Zivkocic, Z.; Vracar, L.; Mitic, V.; Miljkovic, M.; *Serb. J. Elect. Eng.*, **2004**, 89-98.
10. Cai, W.; Fu, C.L.; Gao, J.C.; Zhao, C.X; *Adv. Appl. Ceram.*, **2011**, 110,181-185.
11. Saikat, M.; Mousumi, B.; Siddhartha, M.; Singh, P. K; *J. Aust. Ceram. Soc.*, **2013**, 49 (1), 79 – 83.
12. Nath, A.K.; Medhi, N; *Bull. Mater. Sci.*, **2012**, 35, 847–852.
13. Medhi, N.; Nath, A.K; *J. Mater. Eng. Perform.*, **2013**, 22, 2716-2722.
14. Nath, A.K.; Medhi A; *Indian J phys*. **2014**, Doi: 10.1007/s12648-014-0531-5.
15. Holbert, K. E. Displacement Damage Lecture, Radiation Effects on Materials, Arizona State University, U.S.A., **2006.**
16. Ogundare, F. O.; Olarinoye, I. O; *J. Non-Cryst. Solids*, **2016**, 432, 292-299.
17. Wittels, M.; Sherrill, F. A; *J. Appl. Phys.*, **1957**, 28, 606.
18. Lefkowitz, I; *J. Phys. Chem. Solids*, **1958**, 10, 169-173.
19. Keith, E. H.; Steven, S. M.; Sharif, H. A.; Thomas, H. H.; Dane, R. S. Performance of piezoresistive and piezoelectric sensors in pulsed reactor experiments, Topical Meeting on Nuclear Plant Instrumentation, Controls and Human-Machine Interface Technologies, Columbus, Ohio, **2004.**
20. Ahmadu, U.; Usman, A.B.; Muhammad, A.M.; Isah, K.U; *Process. Appl. Ceram.*, **2016,** 10, 79-85.

21. Onoja, A.; Umar, I.M.; Funtua, I.I.; Dim, L.A.; Elegba, S.B; *Nig. Journ. of Phys*., **1995,** 7, 76-80.
22. Chen, Z.; Yuang-fang, Q.U; *Trans. Nonferrous Met. Soc. China*, **2012**, 22, 2742−2748.
23. Yun, S.; Wang, X.; Li, B.; Xu D; *Solid State Commun*., **2007**, 143, 461–465.
24. Saleem, M., Fang, L., Wakeel, A., Rashad, M., Kong, C. Y; *World J. Condens. Matter Phys.*, **2012**, 2, 10-15.
25. Dash, S.K.; Kant, S.; Danlai, B.; Swain, M.D.; Swain, B.B; *India J. Phys.*, **2014,** 88(2), 129-135.
26. Hsiang, H.-I; Yen, F-S.; Chang Y.-H. *J. Mater. Sci.,* **1996**, 31, 2417-2424.
27. Miclea, C.; Tanasoiu, C.; Miclea, C.F.; Spanulescu, I.; Cioangher, M; *J. Phys. IV France*, **2005**, 128**,** 115–120.
28. Henriques, A.; Graham, J.T.; Landsberger, S.; Ihlefeld, J.F.; Brennecka, G. L.; Brown, D.W.; Forrester, J.S.; Jones, J.L; *AIP Advances* **2014**, 4,117125.
29. Mady, H.A; *Aust. J. Basic Appl. Sci;* **2011**, 5, 1472-1477.
30. Toacsan, M.I.; Ioachin A.; Nedeku, L.; Alexandru, H.V; *Prog. Solid State Chem.*, **2007**, 35, 531-537.
31. Badapanda, T. Structural, Electrical and Optical Study of 'A' Site Deficient Heterovalent Ion Doped Barium Zirconium Titanate Perovskite. Ph. D Dissertation, National Institute of Technology, Rourkela-769008.Orissa India, **2010**.
32. Korkmaz, E.; Kalaycioglu, N.O; *Bull. Mater. Sci.,* **2012**, 35, 1011-1017.

